ELSEVIER

Local structure in the Li-ion battery cathode material Li$_x$(Mn$_y$Fe$_{1-y}$)PO$_4$ for $0 < x \leq 1$ and $y = 0.0$, 0.5 and 1.0

Christopher M. Burba [a,*], Roger Frech [b]

[a] *Department of Natural Sciences, Northeastern State University, 611 N Grand Ave., Tahlequah, OK 74464, USA*
[b] *Department of Chemistry and Biochemistry, University of Oklahoma, 620 Parrington Oval, Room 208, Norman, OK 73019, USA*

Abstract

Infrared and Raman spectroscopy have been used to investigate the Li-ion battery cathode materials Li$_x$(Mn$_y$Fe$_{1-y}$)PO$_4$ for $0 < x \leq 1$ and $y = 0.0$, 0.5 and 1.0. In the Raman spectrum of Li(Mn$_{0.5}$Fe$_{0.5}$)PO$_4$, the frequency of the PO$_4^{3-}$ symmetric stretching mode is very similar to that found in LiFePO$_4$ and LiMnPO$_4$, suggesting that the P–O bond lengths are similar across the entire Li(Mn$_y$Fe$_{1-y}$)PO$_4$ solid-solution series. The more localized ν_1 and ν_3 bands (symmetric and antisymmetric PO$_4^{3-}$ stretching modes, respectively) in the infrared spectra exhibit two-mode behavior for all three Li(Mn$_y$Fe$_{1-y}$)PO$_4$ compositions studied, whereas the PO$_4^{3-}$ antisymmetric bending modes (ν_4) and the Li$^+$ cage mode frequencies vary with Mn^{2+} concentration. The vibrational modes in Li$_x$(Mn$_{0.5}$Fe$_{0.5}$)PO$_4$ are sensitive to lithium content (x) and are, thus, used to investigate changes in the (Mn$_{0.5}$Fe$_{0.5}$)PO$_4$ framework under cycling. The lack of spectral changes during the Fe^{2+}/Fe^{3+} redox couple (3.7 V versus Li$^+$/Li) suggests that the PO$_4^{3-}$ anions have similar local environments in Li(Mn$_{0.5}^{(II)}$Fe$_{0.5}^{(II)}$)PO$_4$ and Li$_{0.5}$(Mn$_{0.5}^{(II)}$Fe$_{0.5}^{(III)}$)PO$_4$. Two-phase behavior is confirmed during the Mn^{2+}/Mn^{3+} redox couple (4.2 V), and the infrared spectrum for (Mn$_{0.5}^{(III)}$Fe$_{0.5}^{(III)}$)PO$_4$ is similar to that of FePO$_4$ since both phases contain PO$_4^{3-}$ anions coordinated only to trivalent transition metal ions. However, the PO$_4^{3-}$ anions are much more distorted in (Mn$_{0.5}^{(III)}$Fe$_{0.5}^{(III)}$)PO$_4$ compared to FePO$_4$, probably as a result of deformation of the MnO$_6$ octahedra induced by Jahn–Teller active Mn^{3+} ions in the (Mn$_{0.5}^{(III)}$Fe$_{0.5}^{(III)}$)PO$_4$ structure. Raman spectra suggest that the carbon layer coating the Li(Mn$_{0.5}$Fe$_{0.5}$)PO$_4$ particles (to improve electronic contact between particles) is predominantly composed of sp^2-hybridized carbon atoms.
© 2007 Elsevier B.V. All rights reserved.

Keywords: Li(Mn,Fe)PO$_4$; Infrared spectroscopy; Raman spectroscopy; Cathodes; Lithium-ion batteries

1. Introduction

Over the past few years, there has been considerable research into developing phospho-olivine LiMPO$_4$ (M = Fe, Mn, Co or Ni) compounds for the next generation of lithium rechargeable batteries. Most of this research effort has been focused on LiFePO$_4$ because of its high theoretical capacity (170 mAh g^{-1}) [1], 3.5 V operating potential versus Li$^+$/Li, excellent coulombic efficiency under optimal conditions [2], and environmentally benign constituents [3]. Lithium extraction occurs in a topotactic two-phase process, whereby Li$^+$ ions are removed from the tryphilite phase (LiFePO$_4$) to form the heterosite phase FePO$_4$ [1,4]. Recently it has been shown that the situation is somewhat

more complicated [5,6]. In the very early stages of delithiation, lithium ions diffuse from the LiFePO$_4$ particles through a single-phase reaction pathway, leaving the cathode with an approximate composition of Li$_{0.97}$FePO$_4$. At this point, lithium extraction becomes two-phase and a shell of lithium-deficient Li$_{0.03}$FePO$_4$ is produced on the surface of the particles. As the cells are further charged, the Li$_{0.03}$FePO$_4$ shell grows inward at the expense of the Li$_{0.97}$FePO$_4$ core. At the end of the charging step, the cathode undergoes a second single-phase reaction to produce FePO$_4$.

In the original studies, only a minor fraction of the theoretical specific capacity was achieved for LiFePO$_4$, especially at higher rates [1]. This was attributed to the diffusion-limited transfer of Li$^+$ ions across the phase boundary of LiFePO$_4$ and FePO$_4$ [1], which is related to the poor intrinsic electronic conductivity of LiFePO$_4$ (between 10^{-9} and 10^{-8} S cm^{-1} at room temperature) [7]. Several approaches have been employed to

---

* Corresponding author. Tel.: +1 918 444 3835; fax: +1 918 458 2325.
E-mail address: burba@nsuok.edu (C.M. Burba).

improve the cycling performance of $LiFePO_4$-based cathodes. One has been to optimize the synthesis conditions so that the formation of Fe^{3+} impurities is suppressed and the particle sizes are minimized. These smaller particles have a larger surface area available for Li^+ (de)intercalation [8]. Other material processing strategies has been to try to increase the effective electronic conductivity of the $LiFePO_4$ electrode to technologically useful levels [9–13]. These efforts include coating the particles with a thin layer of carbon [14].

Phospho-olivine $LiMnPO_4$ has also been investigated as a potential cathode material for lithium rechargeable batteries, since it has a higher operating potential than $LiFePO_4$ (4.1 V versus Li^+/Li) [15–18]. Here, lithium extraction also proceeds according to a two-phase mechanism between $LiMnPO_4$ and $MnPO_4$ [18]. However, the rate capability of this material is very poor compared to $LiFePO_4$ [17]. This may be because $LiMnPO_4$ is an insulator with a $\sim$2 eV spin exchange band gap, whereas $LiFePO_4$ is a semiconductor with a $\sim$0.3 eV crystal field band gap [19]. A number of workers have shown that the Mn^{2+}/Mn^{3+} redox couples can be accessed at reasonable rates by forming the $Li(Mn_yFe_{1-y})PO_4$ solid-solution [1,19–24]. These compounds are isostructural with their $LiFePO_4$ and $LiMnPO_4$ end-members, adopting the same olivine-like structure as $LiFePO_4$: space group *Pnma* (D_{2h}^{16}) [22–24]. The divalent transition metal ions are randomly distributed over $4c$ sites (C_s symmetry). Tetrahedrally coordinated P^{5+} cations are also located on $4c$ sites and bridge the MO_6 chains to form an interconnected three-dimensional structure. The Li^+ ions are octahedrally coordinated and situated on $4a$ sites (C_i symmetry). Lithium (de)intercalation proceeds over two voltage plateaus at 3.5 and 4.1 V, corresponding to the Fe^{2+}/Fe^{3+} and Mn^{2+}/Mn^{3+} redox couples, respectively [1], with the relative length of each plateau depending on the manganese concentration.

The two-dimensional phase diagram of $Li_x(Mn_yFe_{1-y})PO_4$ ($0 \leq x$, $y \leq 1$) has been investigated extensively with X-ray diffraction, X-ray absorption, magnetic susceptibility and Mössbauer techniques [23,25–27]. Yamada et al. reported unusual phase behavior for compounds with intermediate lithium concentrations [23]. Specifically, they noted that the presence of Mn^{2+} ions introduces a single-phase mechanism during the Fe^{2+}/Fe^{3+} redox couple as Li^+ ions are extracted from $Li_x(Mn_yFe_{1-y})PO_4$ [23]. At high Mn^{2+} concentrations, the Fe^{2+}/Fe^{3+} couple proceeds entirely by this single-phase mechanism, while for low Mn^{2+} concentrations, the Fe^{2+}/Fe^{3+} couple is associated with a two-phase followed by a single-phase mechanism. Furthermore, lithium extraction during the Mn^{2+}/Mn^{3+} redox couple is described by a two-phase reaction regardless of manganese concentration. Recently, Bramnik et al. have used high resolution X-ray diffraction to propose two-phase delithiation reactions for both Fe^{2+}/Fe^{3+} and Mn^{2+}/Mn^{3+} redox couples in $Li_x(Mn_{0.6}Fe_{0.4})PO_4$ [28]. However, their data was consistent with a single-phase region $0.55 \leq x \leq 0.67$ in $Li_x(Mn_{0.6}Fe_{0.4})PO_4$ [28].

Although there have been several investigations into the local structure of these $LiMPO_4$ compounds, the majority have used Mössbauer spectroscopy and X-ray absorption spectroscopy to focus on the transition metal ions [4,8,21–27,29,30]. Tucker et

al. utilized ^7Li and ^{31}P magic angle spinning nuclear magnetic resonance (MAS-NMR) to investigate local structure around the Li and P atoms in some $LiMPO_4$ materials [31,32]. A number of researchers have shown that vibrational spectroscopy is very useful in probing fundamental lithium intercalation reactions in a variety of crystalline electrode materials [33–42]. For example, the $LiFePO_4$–$FePO_4$ phase change could be easily identified in Li_xFePO_4 ($0 \leq x \leq 1$) cathodes using vibrational spectroscopy [42]. The vibrational modes of the phosphate anions are expected to be quite sensitive to lithium extraction in $Li(Mn_yFe_{1-y})PO_4$ because the lithium and transition metal ions are coordinated to the oxygen atoms of the covalent P–O bonds in the tetrahedral PO_4^{3-} anions. Thus, a vibrational spectroscopic investigation of the carbon-coated compounds $Li_x(Mn_yFe_{1-y})PO_4$ ($y = 0$, 0.5, 1) compounds will provide a unique perspective on the lithium (de)intercalation reactions accompanying cathode cycling.

2. Experimental methods

Samples of $LiFePO_4$ and $LiMnPO_4$ were received from Kerr-McGee Stored Power Company. Lithium ions were chemically extracted from $LiFePO_4$ using a sufficient quantity of bromine in acetonitrile to form $FePO_4$ [42]. The product was washed thoroughly with acetonitrile and dried overnight under reduced pressure. Samples of $LiFe_{0.5}Mn_{0.5}PO_4$ were prepared by the solid-state reaction of stoichiometric amounts of $FeC_2O_4·2H_2O$, $MnCO_3$, $NH_4H_2PO_4$ and Li_2CO_3. These starting materials were thoroughly mixed and ground together with 4 wt% cellulose acetate. The synthesis was conducted under a flow of nitrogen gas to prevent oxidation of the Fe^{2+} ions. The mixture was slowly heated to 700 °C and annealed for 24 h. The crystal structure was confirmed by X-ray powder diffraction (STOE & Cie GmbH STADI powder diffractometer). Exposures were made in transmission mode with Ge-monochromatized Co $K_{\alpha 1}$ radiation ($\lambda = 1.78897$ Å).

Lithium ions were electrochemically extracted from the carbon-coated $Li(Mn_{0.5}Fe_{0.5})PO_4$ to form the $Li_x(Mn_{0.5}Fe_{0.5})PO_4$ materials. To this end, cathodes were prepared by mixing 87 wt% active material, 5 wt% KS-6 graphitic carbon (TimCal, Ltd.), 5 wt% Super P and 3 wt% Teflon. The resulting mixture was then pressed into a thin sheet. Circular disks were cut from the sheet (0.62 cm^2 and 4.0 ± 0.6 mg) and dried overnight at 150 °C in a vacuum oven. Coin cells were constructed using a lithium metal anode and an electrolyte of 1 M $LiPF_6$ in a 1:1 solution of ethylene carbonate (EC) and diethyl carbonate (DEC). The cell potential was swept potentiostatically between 4.60 and 2.85 V at approximately 55 °C using a 0.5 mV s^{-1} rate. All of the cells were taken through one complete cycle before they were charged to the desired voltage. Afterwards, the cells were disassembled under an argon atmosphere, washed twice in DEC, dried under reduced pressure at room temperature and stored under argon.

Raman scattering experiments were conducted on a Jobin-Yvon ISA T64000 spectrometer in the triple subtractive mode. A 532 nm laser (Spectra-Physics Millennia Vs) was focused onto the surface of the powders through the 80× objective lens of an Olympus microscope, and all of the spectra were recorded in a 180° back-scattering configuration using a CCD detector. The

laser power was set to approximately 10 mW at the laser head to avoid thermal damage to the samples. Transmission FT-IR spectra were recorded at 1 cm^{-1} resolution with a Bruker IFS 66v spectrometer equipped with a KBr beam splitter and a DTGS detector.

3. Results and discussion

3.1. The Raman spectrum of Li(Mn$_{0.5}$Fe$_{0.5}$)PO$_4$

The Raman spectrum of Li(Mn$_{0.5}$Fe$_{0.5}$)PO$_4$ is presented in Fig. 1. Two broad bands at ca. 1595 and 1342 cm^{-1} dominate the spectrum; these bands are due to the carbon coating on the surface of the particles. At the Brillouin zone center, the vibrational modes of crystalline graphite are distributed among the irreducible representations of the D_{6h} point group (A$_{2u}$ + 2B$_{2g}$ + E$_{1u}$ + 2E$_{2g}$) [43]. Only the two E$_{2g}$ modes are Raman-active in first-order scattering experiments [43]. These vibrational modes correspond to the in-plane motion of the carbon atoms and have been observed at 42 and 1581 cm^{-1} (G band) [44]. Several researchers have reported additional bands in the Raman spectrum of microcrystalline graphite between 1318 and 1355 cm^{-1} (D band) and at 1623 cm^{-1} (D' band) [43–46]. These bands are thought to be non-Brillouin-zone-center phonons arising from the crystal boundary regions in the microcrystalline graphite. Tuinstra and Koenig [43] and Nikiel and Jagodzinski [46] have shown that the integrated intensity ratio of the G and D bands is inversely proportional to the intraplane crystallite size, L$_a$, in polycrystalline graphite. The linewidths of the G, D and D' bands are also somewhat dependant on L$_a$ [46].

Doeff et al. characterized a series of carbon-coated LiFePO$_4$ compounds with Raman spectroscopy and determined that the electrochemical discharge capacity depends on the integrated intensity ratio of the D and G bands and on the relative amount of sp^2- and sp^3-hybridized carbon [47]. Materials with a low D/G ratio were predominantly composed of sp^2-type carbon and gave the best electrochemical performance. Wagner et al. [48] and Ramsteiner and Wagner [49] used resonance Raman spectroscopy to probe the relative abundance of sp^2- and sp^3-hybridized carbon in amorphous carbon and microcrystalline graphite. The resonance Raman technique is sensitive to the electronic π–π* transition that occurs between 3.5 and 6.5 eV for sp^2-bonded carbon atoms [48]. Although resonance Raman experiments were not performed on the Li(Mn$_{0.5}$Fe$_{0.5}$)PO$_4$ samples, the bands at 1595 and 1342 cm^{-1} in Fig. 1 closely resemble the bands of carbon-coated LiFePO$_4$ (sample 3A) from Doeff et al. [47] and the microcrystalline graphite, which is predominately sp^2-hybridized carbon, from Wagner et al. [48]. It is therefore reasonable to conclude that the Li(Mn$_{0.5}$Fe$_{0.5}$)PO$_4$ particles have at least a partial coverage of disordered graphite, composed mostly of sp^2-coordinated carbon atoms.

Fig. 1 also contains a weak band at 948 cm^{-1} that is assigned to the A$_g$ mode of the totally symmetric stretching vibrations of the PO$_4^{3-}$ anions (ν_1) for Li(Mn$_{0.5}$Fe$_{0.5}$)PO$_4$. Although its intensity is much weaker than the corresponding bands in other LiMPO$_4$ (M = Mn, Fe, Co and Ni) systems, the frequencies are very similar [42,50–54]. This suggests that the P–O bond lengths in Li(Mn$_{0.5}$Fe$_{0.5}$)PO$_4$ are similar to those in LiFePO$_4$ and LiMnPO$_4$ [55]. The relatively weak intensity of the band in Li(Mn$_{0.5}$Fe$_{0.5}$)PO$_4$ is probably due to the optical skin effect of the carbon-coated Li(Mn$_{0.5}$Fe$_{0.5}$)PO$_4$ particles. Electromagnetic radiation attenuates exponentially as it passes through an absorbing sample, and the effective penetration depth is proportional to the wavelength of the light and the optical constants of the sample [56]. Typically, the penetration depth is between 1/4 and 1/2 of the wavelength of the light. In these experiments, the wavelength of the Raman excitation laser is 532 nm. The laser beam therefore penetrates only a fraction of a micron into the particles, and the scattering volume predominantly contains the carbonaceous surface layer and only a small amount of the Li(Mn$_{0.5}$Fe$_{0.5}$)PO$_4$ material.

3.2. The infrared spectra of Li(Mn$_y$Fe$_{1-y}$)PO$_4$

Infrared spectra of the intramolecular stretching modes (ν_1 and ν_3) for Li(Mn$_y$Fe$_{1-y}$)PO$_4$ ($0 \leq y \leq 1$) are presented in Fig. 2. Spectral assignments for many of the LiMPO$_4$ vibrations have been previously reported in the literature and are assumed here [42,50,54,57]. In general, the infrared spectra of LiFePO$_4$ and LiMnPO$_4$ are very similar. Both compounds have two bands between 1000 and 800 cm^{-1} that are assigned to ν_1, and each spectrum contains three bands at 1138, 1095 and ca. 1060 cm^{-1} belonging to ν_3. The infrared spectrum of Li(Mn$_{0.5}$Fe$_{0.5}$)PO$_4$ exhibits two-mode behavior, whereby the PO$_4^{3-}$ intramolecular stretching region is essentially a superposition of spectra characteristic of the two end-members (LiFePO$_4$ and LiMnPO$_4$), and the relative intensities of the partially overlapping bands are governed by the phase composition of the material [58]. For example, there are two bands at 1067 and 1053 cm^{-1} instead
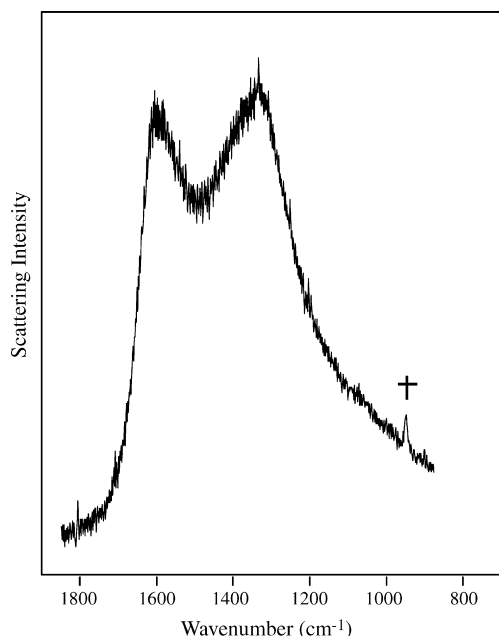

Fig. 1. Raman scattering spectrum of carbon-coated Li(Mn$_{0.5}$Fe$_{0.5}$)PO$_4$. The dagger (†) denotes the A$_g$ mode of ν_1.
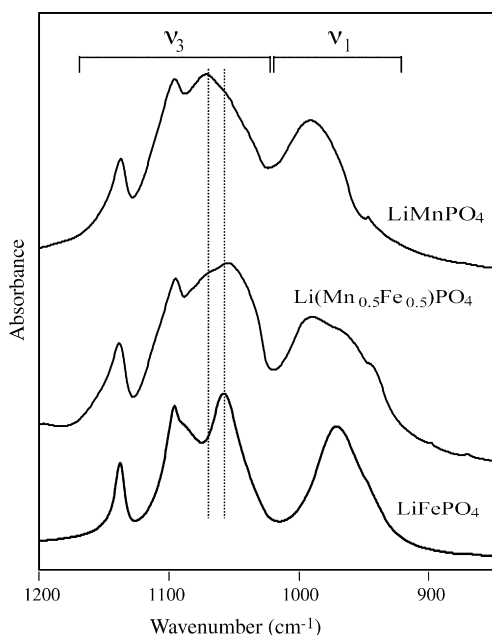
Fig. 2. Infrared absorption spectra of ν_1 and ν_3 for Li(Mn$_y$Fe$_{1-y}$)PO$_4$ ($y = 0$, 0.5, 1). The dashed lines denote the two-mode behavior in ν_3.

of a single band at the mean frequency for Li(Mn$_{0.5}$Fe$_{0.5}$)PO$_4$ (see Fig. 2). This may be contrasted with one-mode behavior, where a broadened single band would be observed throughout the solid-solution series at a frequency that is roughly the weighted average of the frequencies of the end-members [58].

Fig. 3 contains infrared spectra of Li(Mn$_y$Fe$_{1-y}$)PO$_4$ between 700 and 450 cm^{-1}. Four bands ranging in frequency from 550 to 650 cm^{-1} are assigned to antisymmetric PO$_4^{3-}$ bending vibrations (ν_4). The bands near 500 and 465 cm^{-1} are assigned to Li$^+$ ion "cage modes" [50]. In these modes, Li$^+$
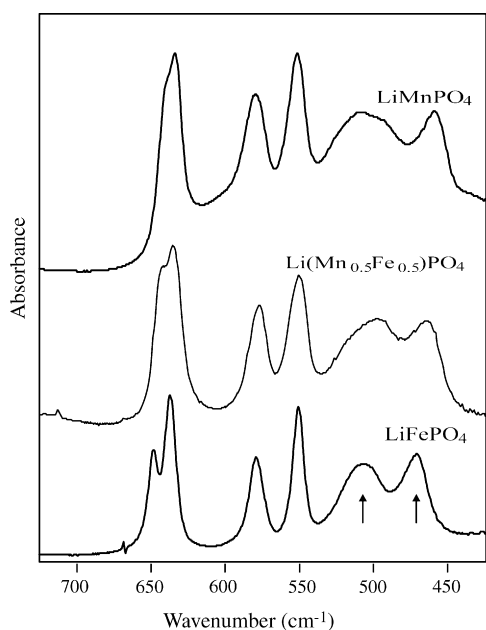
ions undergo translatory motion in an octahedral environment defined by nearest-neighbor oxygen atoms coordinating the Li$^+$ ions. A factor group correlation analysis of the Li$^+$ ion vibrations yields the 12 normal modes at the Brillouin zone center ($3A_u + 3B_{1u} + 3B_{2u} + 3B_{3u}$). These modes are distributed among the irreducible representations of the D_{2h} point group [50]. The modes with A_u symmetry are both Raman- and infrared-inactive; this leaves nine IR-active Li$^+$ ion cage modes in Li(Mn$_y$Fe$_{1-y}$)PO$_4$, which can mix with other vibrational modes of identical symmetry to produce bands representing a complex mixture of atomic motion. However, comparison of the vibrational spectra of LiFePO$_4$ and NaFePO$_4$ suggests that the Li$^+$ ion cage modes are highly decoupled, and the bands near 500 and 465 cm^{-1} consist almost entirely of Li$^+$ ion translatory motion [59].

Unlike the stretching modes in Fig. 2, the lithium cage modes and ν_4 do not exhibit two-mode behavior throughout the Li(Mn$_y$Fe$_{1-y}$)PO$_4$ solid-solution series. Instead, the frequencies of these bands depend on the value of y; for example, the bands at 648 and 637 cm^{-1} in the LiFePO$_4$ spectrum merge and shift to lower frequency for increasing y. Although none of the phosphate vibrations consist only of P and O motion, the PO$_4^{3-}$ bending modes generally contain more M^{2+} (M = Fe or Mn) and Li$^+$ motion than the stretching modes. Thus, ν_1 and ν_3 are more localized than ν_4 and the Li$^+$ cage modes and exhibit two-mode behavior while the lower frequency modes do not [58].

3.3. The infrared spectra of Li$_x$(Mn$_{0.5}$Fe$_{0.5}$)PO$_4$

Fig. 4 shows a cyclic voltammogram of the Li(Mn$_{0.5}$Fe$_{0.5}$)PO$_4$ cells. On the anodic sweep, two peaks appear at 3.7 and 4.2 V, corresponding to the Fe^{2+}/Fe^{3+} and Mn^{2+}/Mn^{3+} redox couples, respectively [1]. The cells typically deliver capacities of 135 mAh g^{-1}. For simplicity, samples charged to 4.6 V are referred to as (Mn$_{0.5}$Fe$_{0.5}$)PO$_4$ even though there is residual lithium in the particles. During the cathodic sweep, Mn^{3+} is reduced to Mn^{2+} at 3.8 V, followed by the reduction of Fe^{3+} to Fe^{2+} at 3.3 V [1].
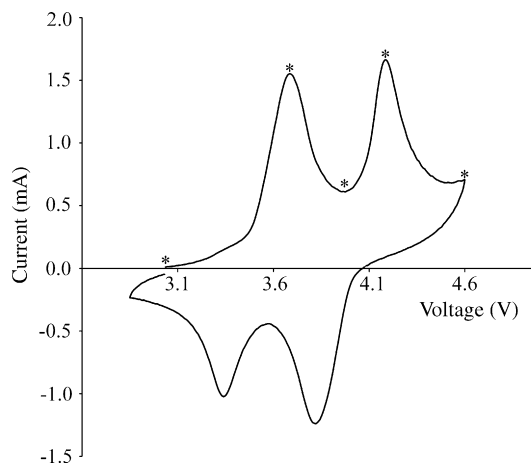

Fig. 3. Infrared absorption spectra of ν_4 and the lithium cage modes for Li(Mn$_y$Fe$_{1-y}$)PO$_4$ ($y = 0$, 0.5, 1). The arrows denote the lithium cage modes.

Fig. 4. Cyclic voltammogram of Li(Mn$_{0.5}$Fe$_{0.5}$)PO$_4$ between 2.85 and 4.6 V (0.5 mV sec^{-1}). The asterisks (*) denote points where cells were disassembled for spectroscopic measurements of the cathode material.
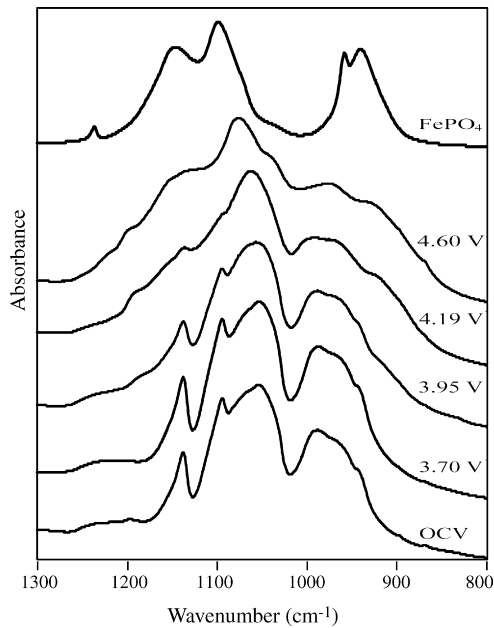
Fig. 5. Infrared absorption spectra of ν_1 and ν_3 for $Li_x(Mn_{0.5}Fe_{0.5})PO_4$ and $FePO_4$ at various states of charge.

Fig. 5 contains infrared absorption spectra in the ν_1 and ν_3 frequency range for $Li_x(Mn_{0.5}Fe_{0.5})PO_4$ cathodes with different Li content, along with $FePO_4$. Only minor spectral changes occur when Fe^{2+} is oxidized to Fe^{3+} (the initial OCV to 4.60 V) in the $Li_x(Mn_{0.5}Fe_{0.5})PO_4$ cathodes. For example, a high frequency shoulder appears on the 1137 cm^{-1} band. However, the ν_1 and ν_3 modes undergo dramatic changes during the Mn^{2+}/Mn^{3+} redox couple (3.95–4.60 V). For instance, the two bands at 1076 and 1040 cm^{-1} replace the asymmetric band near 1060 cm^{-1}, while the three bands at 989, 968 and 944 cm^{-1} collapse into two bands at 972 and 929 cm^{-1}. There are several differences in the vibrational spectra of $(Mn_{0.5}Fe_{0.5})PO_4$ and $FePO_4$. The most intense ν_3 mode of $(Mn_{0.5}Fe_{0.5})PO_4$ is at 1076 cm^{-1}, whereas the band is centered at 1099 cm^{-1} in the spectrum of $FePO_4$. The ν_1 and ν_3 bandwidths are also dependant on Li^+ concentration over the Mn^{2+}/Mn^{3+} redox couple—the $(Mn_{0.5}Fe_{0.5})PO_4$ bands are much broader than the corresponding $FePO_4$ bands.

Similar changes are observed for the ν_4 and Li^+ cage modes in Fig. 6. Only minor spectral changes in the infrared bands are observed during the Fe^{2+}/Fe^{3+} redox couple, but rather dramatic changes occur during the Mn^{2+}/Mn^{3+} couple. For example, the intensity of the 496 cm^{-1} band diminishes slightly when the cells are charged to 3.95 V, but the band at 661 cm^{-1} increases in intensity at the expense of the 642 cm^{-1} band. A new band appears at 532 cm^{-1}, which gradually replaces the 577 and 551 cm^{-1} bands between 3.95 and 4.6 V. Additionally, the 661 and 642 cm^{-1} bands become a single band centered near 650 cm^{-1} in the $(Mn_{0.5}Fe_{0.5})PO_4$ spectrum. The Li^+ cage modes essentially vanish during the Mn^{2+}/Mn^{3+} redox couple, leaving a weak feature near 460 cm^{-1} in the 4.6 V sample. This is possibly due to the residual Li^+ ions in the $(Mn_{0.5}Fe_{0.5})PO_4$ particles.

Bramnik et al. used high resolution synchrotron XRD data to suggest two-phase mechanisms for the Fe^{3+}/Fe^{2+} and $Mn^{3+}/$
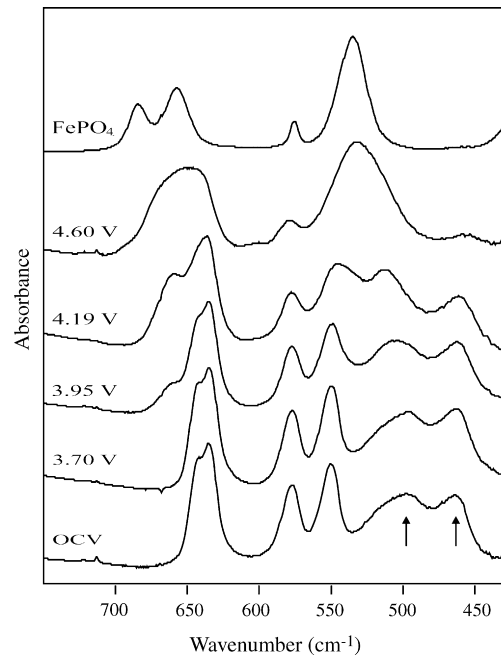

Fig. 6. Infrared absorption spectra of ν_4 and the lithium cage modes for $Li_x(Mn_{0.5}Fe_{0.5})PO_4$ and $FePO_4$ at various states of charge. The arrows denote the lithium cage modes.

Mn^{2+} redox couples of $Li_x(Mn_{0.6}Fe_{0.4})PO_4$ [28]. These two regions are connected by a narrow single-phase regime in the composition domain $0.55 < x < 0.67$. We speculate that each $Li(Mn_yFe_{1-y})PO_4$ two-phase region follows a shell mechanism similar to Li_xFePO_4. Initial delithiation of $Li(Mn_{0.5}Fe_{0.5})PO_4$ is expected to proceed through a short single-phase mechanism to produce $Li_x(Mn_{0.5}Fe_{0.5})PO_4$ with x slightly less than one. The particle surfaces then become encased with a thin layer of $Li_x(Mn_{0.5}^{(II)}Fe_{0.5}^{(III)})PO_4$ ($x \approx 0.5$) that migrates inward at the expense of the lithium-rich $Li_x(Mn_{0.5}Fe_{0.5})PO_4$ core during the Fe^{2+}/Fe^{3+} redox couple. A second single-phase transition connects the Fe^{2+}/Fe^{3+} and Mn^{2+}/Mn^{3+} redox couples at ca. $x = 0.5$. The Mn^{2+}/Mn^{3+} redox couple is characterized by an immiscibility gap between $Li_{0.5}(Mn_{0.5}^{(II)}Fe_{0.5}^{(III)})PO_4$ and lithium-deficient $Li_x(Mn_{0.5}^{(III)}Fe_{0.5}^{(III)})PO_4$. In this domain, the lithium-deficient $Li_x(Mn_{0.5}Fe_{0.5})PO_4$ forms another shell on the surface of the particles, which then migrates inward as the electrode is charged. At the end of the charging step, $(Mn_{0.5}Fe_{0.5})PO_4$ is formed after a third short single-phase mechanism.

Unfortunately, the two-phase mechanism that operates during the Fe^{2+}/Fe^{3+} redox couple cannot be detected with infrared spectroscopy since the spectra undergo small changes. This behavior is quite different from that in the Li_xFePO_4 system, where $FePO_4$ bands appeared early in the delithiation process and continued to increase at the expense of the $LiFePO_4$ bands [42]. Spectral differences between Li_xFePO_4 and $Li_x(Mn_{0.5}Fe_{0.5})PO_4$ at the same level of delithiation must be due to the presence of the Mn^{2+} ions. In $Li(Mn_{0.5}^{(II)}Fe_{0.5}^{(II)})PO_4$, the Mn^{2+} and Fe^{2+} ions are distributed among symmetrically equivalent 4c sites; thus, there are a number of possible coordination environments for the

PO_4^{3-} anions. During the first electrochemical plateau, particles consist of a lithium-rich $Li_x(Mn_{0.5}Fe_{0.5})PO_4$ encased by $Li_x(Mn_{0.5}Fe_{0.5})PO_4$ ($x = 0.5$). The PO_4^{3-} anions are coordinated to Li^+, Mn^{2+} and Fe^{3+} ions in $Li_x(Mn_{0.5}Fe_{0.5})PO_4$ ($x = 0.5$). In contrast, particles of Li_xFePO_4 consist of a $LiFePO_4$ core within a shell of $FePO_4$ [1,4]; in $FePO_4$ the PO_4^{3-} anions are only coordinated to Fe^{3+} ions. The lack of spectral changes in Figs. 5 and 6 suggests that the local structure about the PO_4^{3-} anions in $Li_x(Mn_{0.5}Fe_{0.5})PO_4$ does not change significantly during the Fe^{2+}/Fe^{3+} redox couple. This is probably because the Li^+ and Mn^{2+} ions cause the structural environment of the PO_4^{3-} anions in $Li_{0.5}(Mn_{0.5}^{(II)}Fe_{0.5}^{(III)})PO_4$ to be more similar to that in $Li(Mn_{0.5}^{(II)}Fe_{0.5}^{(II)})PO_4$ than in $FePO_4$.

The two-phase mechanism can be easily discerned with infrared spectroscopy during the Mn^{2+}/Mn^{3+} redox couple (Figs. 5 and 6). Between 3.95 and 4.60 V, several new bands appear and increase in intensity as the Mn^{2+} is oxidized to Mn^{3+}. This behavior is identical to the spectral changes observed for the two-phase delithiation of $LiFePO_4$ [42]. Indeed, the frequencies of the $(Mn_{0.5}^{(III)}Fe_{0.5}^{(III)})PO_4$ modes are very similar to those of $FePO_4$ [42]. This is because of the similar local structure in $(Mn_{0.5}^{(III)}Fe_{0.5}^{(III)})PO_4$ and $FePO_4$ in that both phases contain PO_4^{3-} anions that coordinate only trivalent transition metal ions.

Above 3.95 V, the $(Mn_{0.5}Fe_{0.5})PO_4$ bandwidths become considerably larger than in $FePO_4$. This indicates that there is a higher degree of disorder around the PO_4^{3-} anions in $(Mn_{0.5}Fe_{0.5})PO_4$ than in $FePO_4$. Previous experiments using extended X-ray absorption fine structure measurements have clearly shown that the local structure around the Mn cations becomes distorted when the Mn^{2+} ions oxidize to Mn^{3+} [22,23]. This was attributed to a strong electron–lattice interaction with the Mn^{3+} ions in the $(Mn_yFe_{1-y})PO_4$ materials (Jahn–Teller effect). The O atoms forming the MnO_6 octahedra are covalently bonded to P atoms in the phospho-olivines. Thus, local deformations in the Mn octahedra will directly affect the PO_4^{3-} vibrational modes through the covalent P–O bonds, and result in the significant band broadening observed for the PO_4^{3-} anions in $(Mn_{0.5}Fe_{0.5})PO_4$.

4. Conclusions

The local structure of $Li_x(Mn_yFe_{1-y})PO_4$ was explored by vibrational spectroscopic methods for $0 < x \leq 1$ and $y = 0.0$, 0.5 and 1.0. Raman spectra of the carbon-coated $Li(Mn_{0.5}Fe_{0.5})PO_4$ particles are dominated by two intense bands that are assigned to the G and D bands of graphite. The relative intensities of these bands suggest that the particles are predominately covered with disordered, sp^2-coordinated carbon atoms. The Raman spectrum also contains a weak band at 948 cm^{-1} assigned to the A_g mode of ν_1. The frequency of this band agrees very well with previous Raman spectroscopic measurements of ν_1 in other $LiMPO_4$ phospho-olivine systems [42,50–54,57], indicating that the P–O bond lengths change insignificantly in $Li(Mn_yFe_{1-y})PO_4$ solid solutions [55].

The infrared spectrum of $Li(Mn_{0.5}Fe_{0.5})PO_4$ in the PO_4^{3-} intramolecular stretching region (ν_1 and ν_3) shows two-mode behavior; however the Li^+ cage modes and ν_4 do not exhibit this behavior. Instead, these bands are intermediate between the two end-members ($LiFePO_4$ and $LiMnPO_4$), and the Li^+ cage modes and ν_4 frequencies depend on Mn/Fe composition. The ν_1 and ν_3 vibrations, which exhibit two-mode behavior, are more localized than the ν_4 and Li^+ cage modes.

The PO_4^{3-} vibrations of the $Li(Mn_{0.5}Fe_{0.5})PO_4$ solid-solution are sensitive to lithium extraction, with only minor changes occurring in a few of the bands during the Fe^{2+}/Fe^{3+} redox couple. However, significant changes occur in the PO_4^{3-} vibrations and Li^+ ion cage modes during the Mn^{2+}/Mn^{3+} redox couple. The infrared spectra suggest that the local structure of the PO_4^{3-} anions change insignificantly during the Fe^{2+}/Fe^{3+} redox couple. This is possibly due to the coordination of the PO_4^{3-} anions by Li^+ and Mn^{2+} ions in addition to Fe^{3+}. Moreover, the infrared spectra confirm a two-phase mechanism for the oxidation of Mn^{2+} to Mn^{3+} between 3.95 and 4.60 V. The bandwidths of the $Li_x(Mn_{0.5}Fe_{0.5})PO_4$ ($0 \leq x \leq 0.5$) modes show some dependence on the lithium concentration; the $(Mn_{0.5}Fe_{0.5})PO_4$ bands are much broader than the corresponding bands for $FePO_4$. This indicates that the PO_4^{3-} anions are more disordered in $(Mn_{0.5}Fe_{0.5})PO_4$ compared to $FePO_4$. The local disorder amongst the anions is probably due to local deformations in the MnO_6 octahedra induced by the Jahn–Teller active Mn^{3+} ions in $(Mn_{0.5}Fe_{0.5})PO_4$.

References

[1] A.K. Padhi, K.S. Nanjundaswamy, J.B. Goodenough, J. Electrochem. Soc. 144 (1997) 1188–1194.
[2] K. Zaghib, P. Charest, A. Guerfi, J. Shim, M. Perrier, K. Striebel, J. Power Sources 134 (2004) 124–129.
[3] M.S. Whittingham, Chem. Rev. 104 (2004) 4271–4301.
[4] A.S. Andersson, B. Kalska, L. Häggström, J.O. Thomas, Solid State Ionics 130 (2000) 41–52.
[5] A. Yamada, H. Koizumi, N. Sonoyama, R. Kanno, Electrochem. Solid-State Lett. 8 (2005) A409–A413.
[6] V. Srinivasan, J. Newman, J. Electrochem. Soc. 151 (2004) A1517–A1529.
[7] S.-Y. Chung, J.T. Bloking, Y.-M. Chiang, Nat. Mater. 1 (2002) 123–128.
[8] A. Yamada, S.C. Chung, K. Hinokuma, J. Electrochem. Soc. 148 (2001) A224–A229.
[9] J. Barker, M.Y. Saidi, J.L. Swoyer, Electrochem. Solid-State Lett. 6 (2003) A53–A55.
[10] Z. Chen, J.R. Dahn, J. Electrochem. Soc. 149 (2002) A1184–A1189.
[11] S. Franger, F. Le Cras, C. Bourbon, H. Rouault, Electrochem. Solid-State Lett. 5 (2002) A231–A233.
[12] H. Huang, S.-C. Yin, L.F. Nazar, Eletrochem, Solid-State Lett. 4 (2001) A170–A172.
[13] P.P. Prosini, D. Zane, M. Pasquali, Electrochim. Acta 46 (2001) 3517–3523.
[14] N. Ravet, J.B. Goodenough, S. Besner, M. Simoneau, P. Hovington, M. Armand, 127, Electrochem. Soc. Meet. Abs., Vol. 99-2, Honolulu, HI, October 17–22, 1999.

[15] G. Li, H. Azuma, M. Tohda, Electrochem. Solid-State Lett. 5 (2002) A135–A137.

[16] C. Delacourt, P. Poizot, M. Morcrette, J.-M. Tarascon, C. Masquelier, Chem. Mater. 16 (2004) 93–99.

[17] M. Yonemura, A. Yamada, Y. Takei, N. Sonoyama, R. Kanno, J. Electrochem. Soc. 151 (2004) A1352–A1356.

[18] C. Delacourt, L. Laffont, R. Bouchet, C. Wurm, J.-B. Leriche, M. Morcrette, J.-M. Tarascon, C. Masquelier, J. Electrochem. Soc. 152 (2005) A913–A921.

[19] A. Yamada, M. Hosoya, S.-C. Chung, Y. Kudo, K. Hinokuma, K.-Y. Liu, Y. Nishi, J. Power Sources 119-121 (2003) 232–238.

[20] G. Li, H. Azuma, M. Tohda, J. Electrochem. Soc. 149 (2002) A743–A747.

[21] G. Li, Y. Kudo, K.-Y. Liu, H. Azuma, M. Tohda, J. Electrochem. Soc. 149 (2002) A1414–A1418.

[22] A. Yamada, S.-C. Chung, J. Electrochem. Soc. 148 (2001) A960–A967.

[23] A. Yamada, Y. Kudo, K.-Y. Liu, J. Electrochem. Soc. 148 (2001) A1153–A1158.

[24] A. Yamada, Y. Kudo, K.-Y. Liu, J. Electrochem. Soc. 148 (2001) A747–A754.

[25] A. Yamada, H. Koizumi, N. Sonoyama, R. Kanno, Appl. Phys. Lett., 87 (2006) 252503/252501-252503/252503.

[26] W. Ojczyk, J. Marzec, J. Dygas, F. Krok, R.S. Liu, J. Molenda, Mater. Sci.—Poland 24 (2006) 103–113.

[27] A. Yamada, Y. Takei, H. Koizumi, N. Sonoyama, R. Kanno, Chem. Mater. 18 (2006) 804–813.

[28] N.N. Bramnik, K.G. Bramnik, K. Nikolowski, M. Hinterstein, C. Baehtz, H. Ehrenberg, Electrochem. Solid-State Lett. 8 (2005) A379–A381.

[29] S. Okada, S.-I. Sawa, Y. Uebou, M. Egashira, J.-I. Yamaki, M. Tabuchi, H. Kobayashi, K. Fukumi, H. Kageyama, Electrochemistry 71 (2003) 1136–1138.

[30] O. Haas, A. Deb, E.J. Cairns, A. Wokaun, J. Electrochem. Soc. 152 (2005) A191–A196.

[31] M.C. Tucker, M.M. Doeff, T.J. Richardson, R. Fiñones, J.A. Reimer, E.J. Cairnes, Electrochem. Solid-State Lett. 5 (2002) A95–A98.

[32] M.C. Tucker, M.M. Doeff, T.J. Richardson, R. Fiñones, E.J. Cairns, J.A. Reimer, J. Am. Chem. Soc. 124 (2002) 3832–3833.

[33] E. Cazzanelli, G. Marriotto, S. Passerini, F. Decker, Solid State Ionics 70–71 (1994) 412–416.

[34] E. Cazzanelli, E. Mariotto, S. Passerini, W.H. Smyrl, J. Non-cryst. Solids 208 (1996) 89–98.

[35] W. Huang, R. Frech, J. Electrochem. Soc. 145 (1998) 765–770.

[36] W. Huang, R. Frech, J. Power Sources 81–82 (1999) 616–620.

[37] T. Itoh, H. Sato, T. Nishina, T. Matue, I. Uchida, J. Power Sources 68 (1997) 333–337.

[38] C. Julien, C. Perez-Vicente, G.A. Nazri, Ionics 2 (1996) 468–473.

[39] C. Julien, M. Massot, C. Perez-Vicente, E. Haro-Poniatowski, G.A. Nazri, A. Rougier, Mater. Res. Soc. Symp. Proc. 496 (1998) 415–420.

[40] T.J. Richardson, S.J. Wen, K.A. Striebel, P.N. Ross Jr., E.J. Cairns, Mater. Res. Bull. 32 (1997) 609–618.

[41] A. Šurca, B. Orel, Electrochim. Acta 44 (1999) 3051–3057.

[42] C.M. Burba, R. Frech, J. Electrochem. Soc. 151 (2004) A1032–A1038.

[43] F. Tuinstra, J.L. Koenig, J. Chem. Phys. 53 (1970) 1126–1130.

[44] K. Sinha, J. Menédez, Phys. Rev. B 41 (1990) 10845–10847.

[45] R.J. Nemanich, S.A. Solin, Phys. Rev. B 20 (1979) 392–401.

[46] L. Nikiel, P.W. Jagodzinski, Carbon 31 (1993) 1313–1317.

[47] M. Doeff, Y. Hu, F. McLarnon, R. Kostecki, Electrochem. Solid-State Lett. 6 (2003) A207–A209.

[48] J. Wagner, M. Ramsteiner, C. Wild, P. Koidl, Phys. Rev. B 40 (1989) 1817–1824.

[49] M. Ramsteiner, J. Wagner, Appl. Phys. Lett. 51 (1987) 1355–1357.

[50] M.T. Paques-Ledent, P. Tarte, Spectrochim. Acta 30A (1974) 673–689.

[51] O. García-Moreno, M. Alvarez-Vega, F. García-Alvarado, J. García-Jaca, J.M. Gallardo-Amores, M.L. Sanjuán, U. Amador, Chem. Mater. 13 (2001) 1570–1576.

[52] V.I. Fomin, V.P. Gnezdilov, V.S. Kumosov, A.V. Pechanskii, A.V. Yeremenko, Low Temp. Phys. 28 (2002) 203–209.

[53] V.I. Fomin, V.P. Gnezdilov, V.S. Kumosov, A.V. Peschanskii, V.V. Eremenko, S. Gentil, J.-P. Rivera, Low Temp. Phys. 25 (1999) 829–832.

[54] W. Paraguassu, P.T.C. Freire, V. Lemos, S.M. Lala, L.A. Montoro, J.M. Rosolen, J. Raman Spectrosc. 36 (2005) 213–220.

[55] L.D. Popovic, D. de Waal, J.C.A. Boeyens, J. Raman Spectrosc. 36 (2005) 2–11.

[56] M. Born, E. Wolf, Principles of optics: electromagnetic theory of propagation, in: Interference and Diffraction of Light, fourth ed., Pergamon Press, Oxford, 1970, p. 614.

[57] A.A. Salah, P. Jozwiak, J. Garbarczyk, K. Benkhouja, K. Zaghib, F. Gendron, C.M. Julien, J. Power Sources 140 (2005) 370–375.

[58] P. Tarte, A. Rulmont, M. Liégeois-Duykaerts, R. Cahay, J.M. Winand, Solid State Ionics 42 (1990) 177–196.

[59] C.M. Burba, R. Frech, Spectrochim. Acta A, in press.